Hindawi
Journal of Nanomaterials
Volume 2020, Article ID 8509380, 11 pages
https://doi.org/10.1155/2020/8509380

Research Article

Morphology Manipulation and Upconversion Luminescence Enhancement of β-$NaLuF_4$: Er^{3+} Hexagonal Microtubes via Sr^{2+} Doping

Han Lin, Zhonggen Wang, and Yan Hong

School of Electrical and Information Engineering, Anhui University of Science and Technology, Huainan, 232001 Anhui, China

Correspondence should be addressed to Han Lin; iyishuihan@126.com

Received 11 May 2020; Revised 15 July 2020; Accepted 21 July 2020; Published 28 August 2020

Academic Editor: Hiromasa Nishikiori

A new and facile strategy to enhance the upconversion luminescence (UCL) emission of $NaLuF_4$: Er^{3+} microcrystals (MCs) using strontium (Sr) as a dopant has been reported. With the introduction of Sr^{2+}, the products change from long $NaLuF_4$: Er^{3+} hexagonal microtubes to short hexagonal microtubes and finally to hexagonal microprisms. The growth mechanism is profoundly discussed according to the different reaction time-dependent morphologies. More importantly, the total fluorescence intensity is significantly reinforced by doping Sr^{2+} ions. When 18% Sr^{2+} is doped into $NaLuF_4$: Er^{3+} hexagonal microtubes, the maximum green and red luminescence intensities are about 5.8 and 4.4 times higher than those of Sr^{2+}-free samples, respectively. The influences of Sr^{2+} ion doping content on the phase, the morphology, and the local crystal field symmetry of the as-synthesized $NaLuF_4$ crystals are investigated.

1. Introduction

Upconversion (UC) micro- and nanocrystals refer to a nonlinear optical process in which lower-energy photons are absorbed and higher-energy photons are emitted [1]. In the past few decades, countless scientific researches about trivalent lanthanide ion- (Ln^{3+}-) doped UC materials have aroused widespread attention owing to their applications in many promising fields, such as photovoltaic cells, biological detection, temperature sensing, DNA detection, and photodynamic therapy (PDT) [2–10]. As a typical upconversion matrix material, $NaYF_4$ crystal has attracted much attention due to its low phonon energy (<350 cm^{-1}), long luminescence lifetime, and high thermal stability and has been widely studied [6, 10–14]. The crystal structure of $NaLuF_4$ is similar to $NaYF_4$, with a smaller ion radius (Y^{3+} = 0.89 Å, Lu^{3+} = 0.86 Å), and it is also considered an ideal substitute for the ideal UC matrix [15–20]. Especially Lu^{3+} in $NaLuF_4$ could sensitize the activator and perform volume compensation, resulting in enhanced emission. Despite these advantages, there are still some insurmountable problems. In particular, the efficiency is low, which limits its application to a certain extent for $NaLnF_4$ compounds. Therefore, it is imperative to enhance the luminescent intensity of UC crystal.

It is generally believed that the UC emission of Ln^{3+}-doped materials depends on the internal 4*f* transition probabilities, which is significantly impacted by the local crystal field symmetry of Ln^{3+} ions [21]. Doping impurity ions is an effective way to improve optical performance, which is dependent on local symmetrical tailoring, surface passivation, and surface-plasmon coupling [22, 23]. In particular, alkaline earth ion (Li^+, K^+, Mg^{2+}, Ba^{2+}, and Ca^{2+}) or trivalent Ln^{3+} ion doping methods have already been proved to benefit from modifying the morphology and crystallographic phase of UC crystals. In previous studies, Wang and coworkers studied the effect of Li^+ dopant on $NaYF_4$: Yb^{3+}, Er^{3+} nanocrystals. They observed 34-time green and 101-time red emission enhancement and proposed that UC enhancement could be attributed to local crystal field distortion or disrupted local crystal field symmetry around rare-earth ions [24]. Zhou et al. claimed that by introducing Ca^{2+} ions, the β-$NaLuF_4$: Yb^{3+}/Er^{3+}, Er^{3+}/Tm^{3+} microcrystals could be resized simultaneously and realize green and red emission enhancement by 7.5 and 7.9 times, respectively [25]. Shao

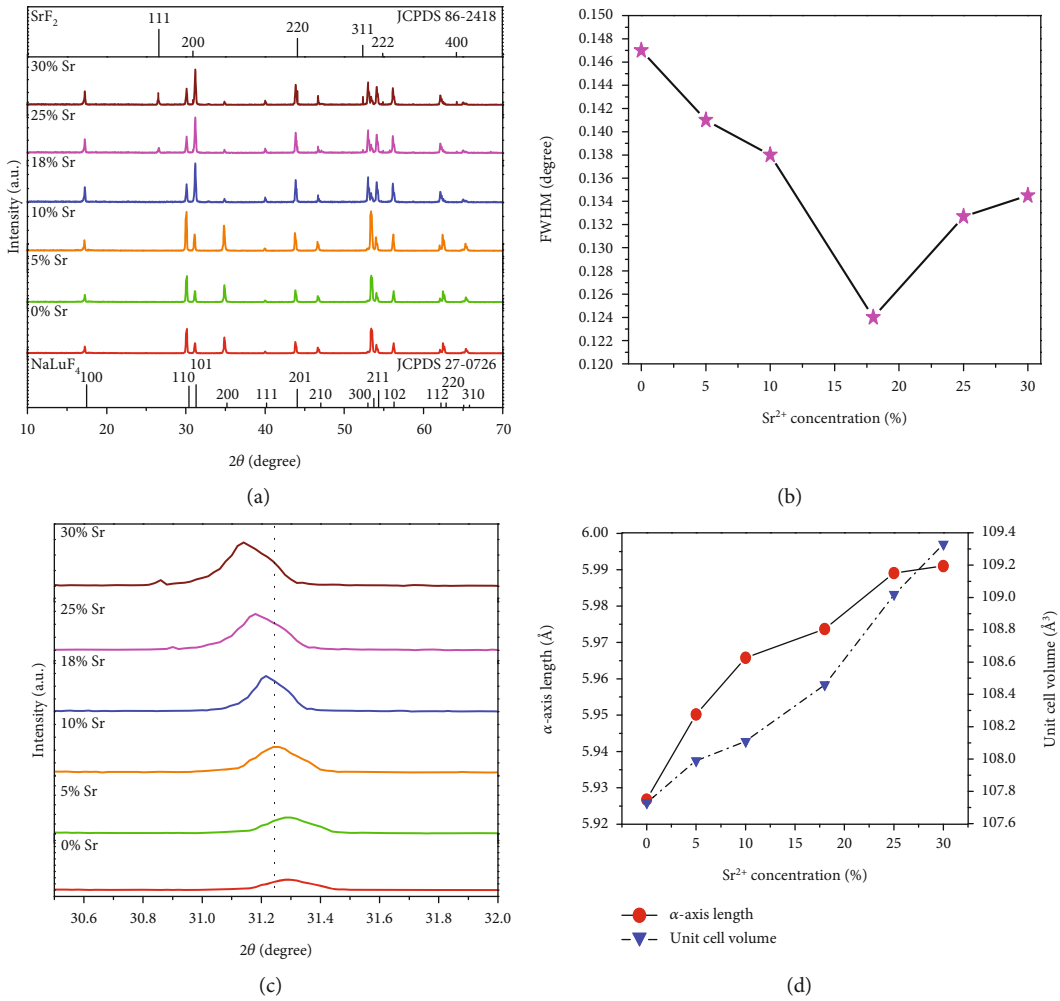

FIGURE 1: (a) XRD patterns of the as-prepared $NaLuF_4$:6%Er^{3+}, x% Sr^{2+} (x = 0, 5, 10, 18, 25, 30) microcrystals. The vertical black lines are the standard profiles of β-$NaLuF_4$ (JCPDS 27-0726) and SrF_2 (JCPDS 86-2418). (b) FWHM of the 31.2° peak vs. content of Sr^{2+} ions. (c) The enlarged view at $2\theta = 31.2°$. (d) Variation trend of the a-axis length and cell volume of the β-$NaLuF_4$:6%Er^{3+} samples doped with different Sr^{2+} contents.

and coworkers doped Ca^{2+} into $NaYF_4$: Nd^{3+} microcrystal, and the near-infrared luminescence intensity at 1.06 μm increased by about three times [26]. Furthermore, doping some special ions could not only improve the luminescence performance but also modify the morphology. Huang and coworkers reported that Sr^{2+} and Tb^{3+} codoping could regulate the size and morphology of $NaCeF_4$ nanorods and Sr^{2+} doping can tune the emission intensity of Tb^{3+}-doped $NaCeF_4$ nanocrystals [27]. These investigations have proved that cationic doping can change electron distribution density and can control the phase transition, morphology, and luminescence intensity of microcrystals or nanocrystals. However, there have been few systematic studies focusing on the structure, morphology, and luminescence of $NaLuF_4$: Er^{3+} microcrystals by Sr^{2+} doping.

Considering the above points, we incorporate Sr^{2+} as a dopant ion into $NaLuF_4$: Er^{3+} for adjusting the local coordination symmetry of Ln^{3+} ions, thereby enhancing the emission efficiency of UC. Through XRD, TEM, and UC emission spectrum characterization analysis, the phase structure, morphology evolution, and UC luminescence property are studied. The results illustrate that, at low concentration of Sr^{2+}, the morphology tended to be hexagonal microtubes with scrappy ends, while high concentration of Sr^{2+} induced the generation of a prism-shaped morphology. Growth process reveals that Sr^{2+}-doped $NaLuF_4$: Er^{3+} hexagonal microtubes are obtained by oriented attachment and Ostwald ripening. Ostwald ripening refers to the growth of larger particles with the help of smaller particles. The main reason is that particles with larger size and smaller surface to volume ratio are better than smaller particles with less energy stability. In addition, it is found that doping Sr^{2+} ions into $NaLuF_4$: Er^{3+} induced effective reinforcement. When 18% Sr^{2+} is doped into $NaLuF_4$: Er^{3+}, the green and red luminescence intensities increase by 5.8 and 4.4 times, respectively. A plausible mechanism for boosting UC luminescence of the synthesized microcrystals is discussed.

2. Experimental

2.1. Materials. Lutetium oxide (Lu_2O_3, 99.999%) and erbium oxide (Er_2O_3, 99.999%) were purchased from Beijing Lansu

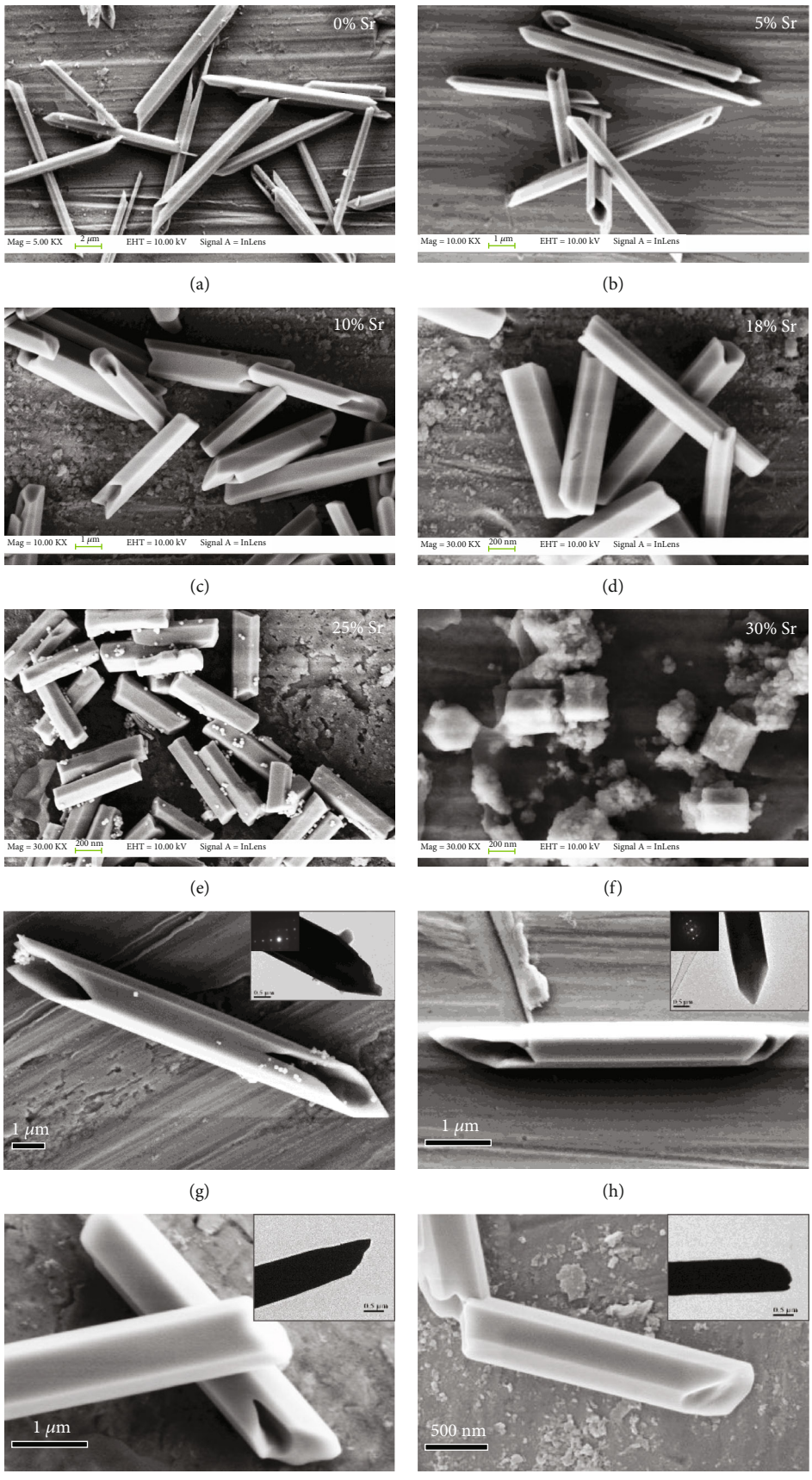

Figure 2: Continued.

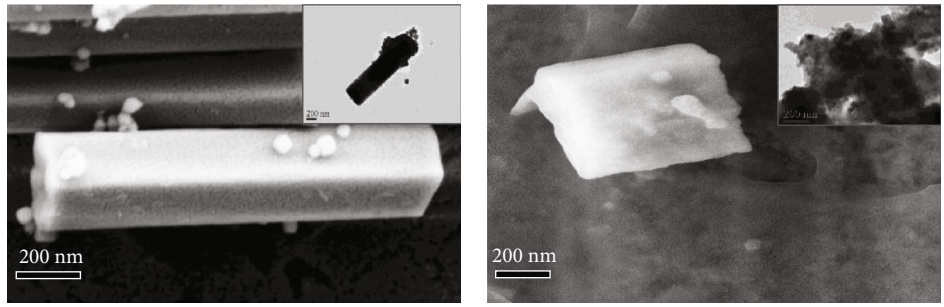

(k) (l)

Figure 2: SEM images of β-$NaLuF_4$:$6Er^{3+}$ MCs doped with Sr^{2+} at different concentrations. (a–f) Refer to 0, 5, 10, 18, 25, and 30%, correspondingly. (g–l) Are corresponding high-resolution SEM images of the microstructures, and insets are TEM images.

Co. China. Sodium fluoride (NaF, AR), $Sr(NO_3)_2$, polyvinylpyrrolidone (PVP-K30), and ethanol (AR) were provided by Sinopharm Chemical Reagent Co. Ltd. The metal oxides were dissolved in 10% hydrochloric solution at elevated temperature and then completely evaporated to prepare the corresponding rare-earth chlorides ($LnCl_3$, Ln: Lu/Er). All of the chemicals were used as received without further refinement. Deionized water was used throughout the experiment.

2.2. Experimental Section

2.2.1. Preparation of Different Sr^{2+}-Doped β-$NaLuF_4$:6%Er^{3+} Micromaterials. Firstly, based on the stoichiometric ratio, 0.2234 g PVP-K30 was dissolved by magnetic agitation in 18 mL distilled water to form a solution of desired molar concentration and 10 mL of an aqueous solution containing certain stoichiometric amounts of $LnCl_3$ (Ln = Lu and Er), $Sr(NO_3)_2$, and NaF was added dropwise into the above mixture. The precursor solution was magnetically stirred for 10 min, then transferred to a 60 mL Teflon-lined autoclave and hydrothermally treated at a temperature at 195°C for 24 h. After hydrothermal treatment, the autoclave was naturally cooled to room temperature. The products were washed alternately with deionized water and ethanol to remove impurities and excessive surfactant, collected by centrifugation, and then dried at 80°C for 8 h for further characterization. Similarly, the same synthesis procedure was used for different Sr^{2+}-doped $NaLuF_4$:6%Er^{3+} microtubes through adding the $Sr(NO_3)_2$ with different concentrations.

2.2.2. Preparation of Sr^{2+}-Doped β-$NaLuF_4$:6%Er^{3+} Micromaterials at Different Durations. In the time-dependent experiment, the addition of Sr^{2+} ions was defined as 10%. The only difference was that the hydrothermal reaction times were performed for 0.5 h, 2 h, 5 h, and 12 h to achieve shape evolution.

2.3. Characterizations. Structures of the as-prepared samples were identified by an X-ray diffractometer (XRD, Ultima-III) using Cu-K_α radiation ($\lambda = 0.15405$ nm). The morphological behavior of final compounds was monitored by a Hitachi S-3400N field emission scanning electron microscope (FE-SEM) and a JEOL JEM-200CX transmission electron microscope (TEM) equipped with an energy-dispersive X-ray spectroscope (EDS). The photoluminescence spectra

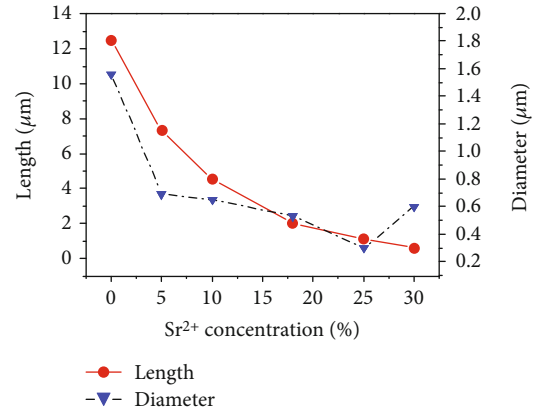

Figure 3: The size evolution of $NaLuF_4$:6%Er^{3+} MCs.

were recorded on a FLS920 spectrofluorimeter equipped with a power-controllable 980 nm diode laser. To compare the emission intensities between different samples, the emission spectra were measured under the same parameters.

3. Results and Discussion

3.1. XRD Analysis. The crystallinity and phase purity of the as-prepared $NaLuF_4$:6%Er^{3+} micromaterials by Sr^{2+} doping at different concentrations (0, 5, 10, 18, 25, and 30%) are presented in Figure 1(a). As Sr^{2+} doping concentration rises from 0 to 10%, all the distinct diffraction peaks in the patterns can be easily labelled as hexagonal phase $NaLuF_4$ (JCPDS 27-0726). No other impurity peak is detected, indicating the good crystallinity of these samples. Compared with the standard peaks, an enhanced intensity of peak at (110) about 30.3° can be observed. The enhancement of the peak indicates that the crystal has preferential growth in this direction. It should be noticed that the (101) diffraction peak about 31.2° became higher than the (110) diffraction peak as the concentration of Sr^{2+} increases up to 18%, which indicates the presence of preferred orientation growth under different Sr^{2+} doping concentrations. It is worth noting that when the Sr^{2+} concentration was further increased to 25%, an impurity, which is the strontium fluoride (SrF_2) phase (JCPDS No. 86-2418), appears.

It can be seen from Figure 1(b) that as the concentration of Sr^{2+} increases to 18%, the full width at half maximum

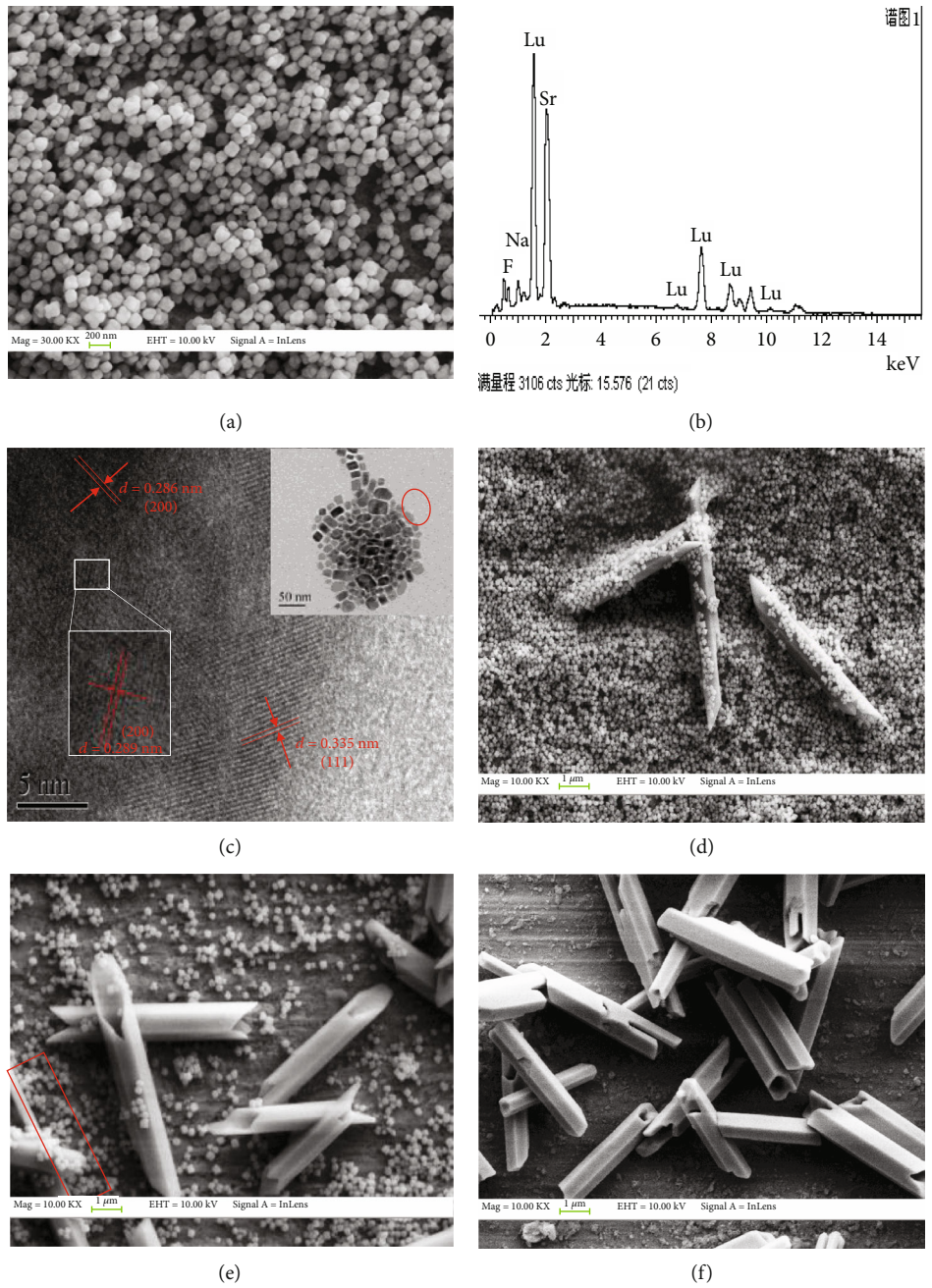

Figure 4: SEM images and corresponding HRTEM images and EDS analysis of intermediate products with different reaction time: (a–c) 0.5 h, (d) 2 h, (e) 5 h, and (f) 12 h.

(FWHM) of the diffraction peak becomes narrower and then widens rapidly when the concentration of Sr^{2+} further increases to 30%. Narrow FWHM means good crystallinity; therefore, when Sr^{2+} doping concentration is less than 18%, the crystallinity increases; and when Sr^{2+} doping concentration is more than 18%, the crystallinity decreases. The magnified XRD patterns in the vicinity of $2\theta = 31.2^{\circ}$ are shown in Figure 1(c). The peak shifts toward a smaller angle with more and more Sr^{2+} doping, indicating that the spacing of crystal planes increases and the lattice expands. Based on the Bragg equation [15, 25],

$$2d \sin\theta = n\lambda, \quad (1)$$

where n is a positive integer, d is the interplanar spacing of the diffracting planes, λ is the incident wavelength, and θ is the intersection angle. Since the ionic radius of Sr^{2+} (1.18 Å) is larger than that of Lu^{3+} (0.86 Å) and Na^{+} (1.02 Å) ions, replacing Lu^{3+} and Na^{+} by Sr^{2+} would enlarge the lattice. The similar phenomenon is also observed in the Ca^{2+}-doped $NaLuF_4$: Yb^{3+}, Er^{3+}, Er^{3+}/Tm^{3+} microcrystals [25]. To probe and detect the variation of the crystal structure

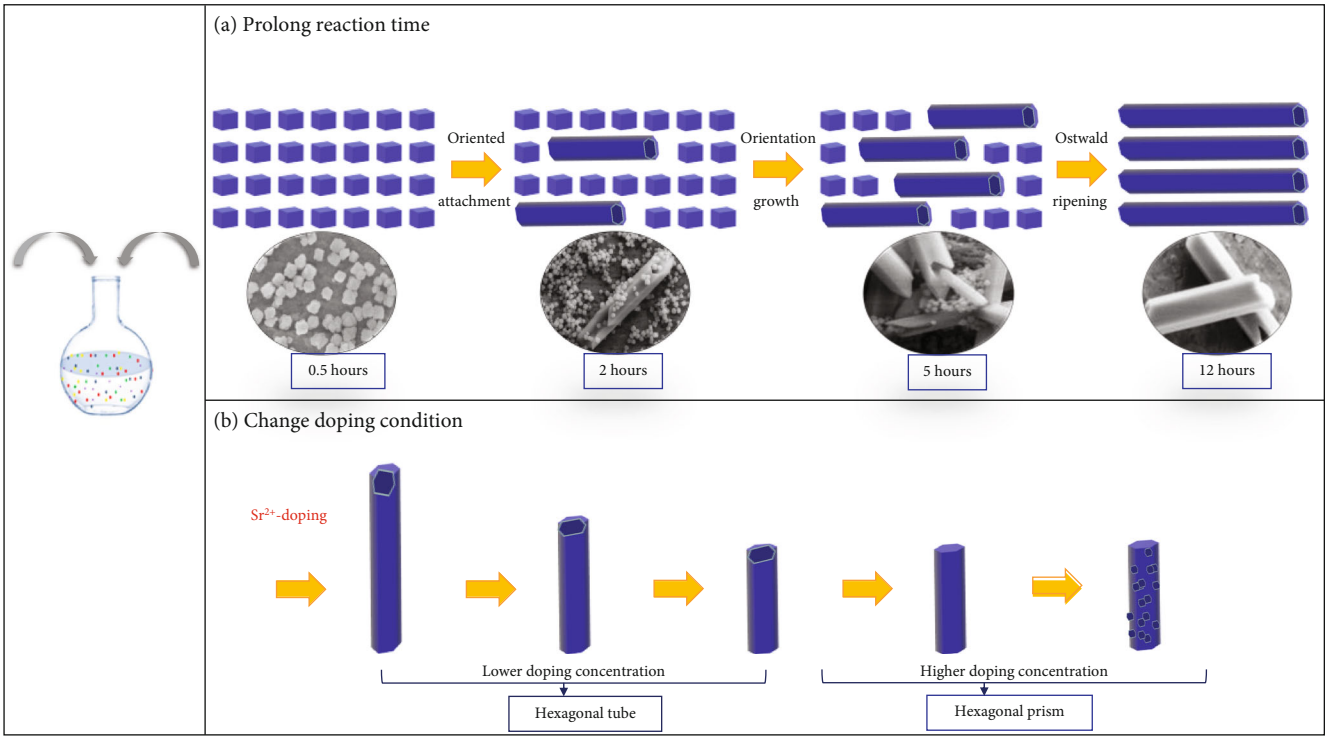

FIGURE 5: Sketch map of the crystal growing process: (a) as-obtained products reacted with different time; (b) doping with different contents of Sr^{2+} as the reaction time is 24 h.

under different Sr^{2+} contents, MC samples prepared with different Sr^{2+} contents were characterized by XRD. Unit cell volume and structural parameters were visually depicted in Figure 1(d). It turns out as expected that the *a*-axis length and unit cell volume increase gradually with the increase of Sr^{2+} doping concentration. Sr^{2+} doping can alter the lattice parameter and plays an essential role in the control of UC luminescence emission.

3.2. Morphology Study

3.2.1. Morphology Evolution of β-$NaLuF_4$:6%Er^{3+} Microcrystals via Sr^{2+} Doping. The corresponding SEM images of Sr^{2+}-doped β-$NaLuF_4$:6%Er^{3+} microcrystals at different concentrations (0, 5, 10, 18, 25, and 30%) are shown in Figures 2(a)–2(f). Figures 2(g)–2(l) are the high-magnification SEM images corresponding to the microstructures, and insets are TEM images. As can be seen from Figure 2(a), the Sr^{2+}-free sample is composed of microtubes. Most of the microtubes have scrappy ends, thin-walled tube, and nanoparticles on the surfaces disorderly and unsystematic. When Sr^{2+} doping is 5%, the hexagonal structure can be observed on the upper and lower surfaces of microtubes with improved ends and smooth surfaces, as exhibited in Figure 2(b), which is in good agreement with the TEM image. When Sr^{2+} doping increases to 10%, the length decreases much. Homogeneous short hexagonal tubes are present in Figure 2(c). When the Sr^{2+} doping concentration varied from 10% to 18%, it can be seen from Figure 2(d) that the walls of hexagonal microtubes are getting thicker and thicker, and the morphology changes to hexagonal microprisms with uniformity and concave centers on the upper and lower surfaces. The internal structure of the microcrystals cannot be detected in the TEM images of Figures 2(i) and 2(j) due to its large thickness. Besides, when the Sr^{2+} content exceeds 25%, the surface of hexagonal prisms is becoming rougher and rougher. According to XRD results, it belongs to the SrF_2 crystal. If Sr^{2+} doping gets to 30%, the flocculent structure appears on the surface of hexagonal prisms (Figure 2(f).

Upon careful checking, as the Sr^{2+} concentration increases from 0 to 5, 10, 18, 25, and 30%, the average length of the corresponding $NaLuF_4$:6%Er^{3+} MCs is 12.5, 7.33, 4.52, 2.01, 1.12, and 0.6 μm, and the average diameter is 1.56, 0.69, 0.65, 0.53, 0.3, and 0.6 μm, respectively. The size evolution (Figure 3) of $NaLuF_4$:6%Er^{3+} microcrystals may be attributed to the significant influence of Sr^{2+} dopant on the crystal growth rate. As the Sr^{2+} ion increases, the phases change from the pure β-$NaLuF_4$ to the mixture of β-$NaLuF_4$ and SrF_2 is achieved. The shape of $NaLuF_4$:6%Er^{3+} is modified from pure hexagonal microtubes to hexagonal prisms with irregular particles.

3.2.2. Growth Mechanism of $NaLuF_4$ Hexagonal Microtubes via Sr^{2+} Doping. To elucidate the growth process of $NaLuF_4$ hexagonal microtubes, intermediate products with different durations (0.5 h, 2 h, 5 h, and 12 h) are obtained, and the doping amount of Sr^{2+} is fixed at 10%. According to the morphologies, the growth process is divided into four stages: (1) nucleation, (2) oriented attachment, (3) orientation growth, and (4) Ostwald ripening. In the first stage, the precursor after 0.5 h reaction is ultrasmall nanoparticles with a cubic morphology, as shown in Figure 4(a). Accordingly, the EDS

results in Figure 4(b) demonstrate the presence of Sr^{2+}, Lu^{3+}, and Na^{+}, where Lu^{3+} content is the maximum and Na^{+} content is the minimum. Therefore, SrF_2 may first nucleate stably and then add Lu^{3+} and Na^{+} into the crystal lattice of SrF_2 nucleus. The product after 0.5 h reaction is SrF_2. From the high-resolution TEM images of some cubic nanocrystals in Figure 4(c), the lattice fringes of 0.286 nm, 0.289 nm, and 0.335 nm are detected, respectively, corresponding to (111) and (220) planes of SrF_2 (JCPDS 86-2418). In the second stage, when the reaction time reaches 2 h, the nanoparticles aggregate together to form aggregates at the microscopic level, which means oriented attachment. Most of the products are still SrF_2 nanocrystals, and some $NaLuF_4$ hexagonal microtubes can be observed from Figure 4(d), and the hexagonal microtubes may originate from the oriented attachment of ultrasmall cubic nanocrystals and have similar morphology with the final product. In the third stage, when the reaction time is prolonged to 5 h, the larger structure starts to grow into $NaLuF_4$ hexagonal microtubes, as shown in Figure 4(e). It is observed in the red rectangle of Figure 4(e) that many SrF_2 nanocrystals align together and intend to fabricate to a new hexagonal tube via orientation growth. When the hexagonal tubes grow to a certain number, the growth process enters the fourth stage. At this stage, at least after 12 h reaction, pure $NaLuF_4$ can be obtained as shown in Figure 4(f).

Based on the above results, we propose the possible modification mechanism of Sr^{2+} doping on the size and morphology of the $NaLuF_4$ MCs, as schematically shown in Figure 5. As the reaction continues, the Ostwald ripening process dominates the growing process. When the cubic nanocrystals with high surface energy are redissolved, Ostwald ripening begins. Hexagonal microtubes are synthesized following the precursor of Lu^{3+} and Sr^{2+} exhausted, and then Sr^{2+}-doped $NaLuF_4$ hexagonal microtubes can be obtained ultimately. On the other hand, at a low concentration of Sr^{2+}, the length of $NaLuF_4$ hexagonal microtubes decreases, while a high concentration of Sr^{2+} induces the generation of a prism-shaped morphology.

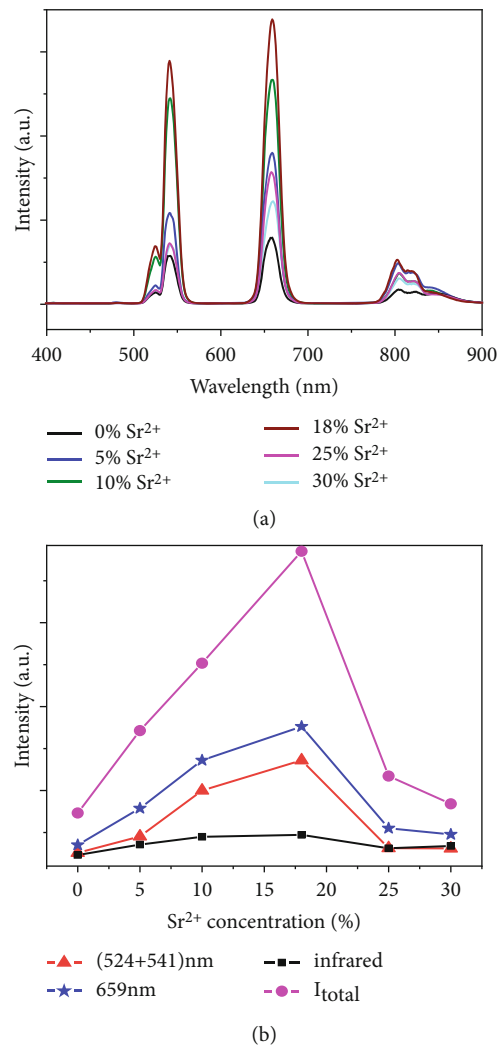

FIGURE 6: (a) The upconversion emission spectra; (b) the integrated intensity variation of green, red, infrared, and all emissions of 6%Er^{3+}, x% Sr^{2+} samples with $x = 0$, 5, 10, 18, 25, and 30 under 980 nm excitation (color figure online).

3.3. Sr^{2+} Induced UCL Modulation and Mechanism Analysis. Figure 6(a) illustrates the UCL spectra of $NaLuF_4$:6%Er^{3+} microcrystals doped by different amounts of Sr^{2+} ions under excitation of a 980 nm continuous wave laser diode. Three distinct visible emission bands can be observed in the range of 500-700 nm. Two green emissions at 505-529 nm and 529-569 nm are assigned to the (Er^{3+}) $^2H_{11/2}\rightarrow{}^4I_{15/2}$, (Er^{3+}) $^4S_{3/2}\rightarrow{}^4I_{15/2}$ transitions, respectively. The red emission from 628 to 692 nm is attributed to the (Er^{3+}) $^4F_{9/2}\rightarrow{}^4I_{15/2}$ transition. Additionally, the infrared emission bands in the range of 700-900 nm can also be found. Sr^{2+} has no obvious energy transfer to RE^{3+} ions. Obviously, in the case of Sr^{2+} doping, both the peak positions and profiles of the emission bands are unaltered. The only difference is the UC emission intensity. It is interesting to observe that when the doping concentration of Sr^{2+} increases from 0 to 18%, the UC emission intensity is initially strengthened and then exhibits an abrupt decrease when the Sr^{2+} amount surpasses 18%. Noticeably, the maximum intensity of the 505-569 nm and 628-692 nm emissions of 18% Sr^{2+}-doped microcrystals is reinforced by 5.8 and 4.4 times, as shown in Figure 6(b).

The enhancement of the upconversion emission efficiency caused by Sr^{2+} doping may be attributed to three aspects: phase, crystal field symmetry, and morphology. Firstly, it is commonly recognized that good crystallinity is beneficial to the luminescence of lanthanide activators. According to the aforesaid XRD data, doping with Sr^{2+} improves the crystallinity of β-$NaLuF_4$:6%Er^{3+} microcrystals. From Figure 1(b), which exhibits the variation of FWHM with Sr^{2+} amount, doping 18% Sr^{2+} ion is the optimum concentration and can improve the crystallinity very well. Significantly, the trend of improved crystallinity well agreed with the trend of enhanced UC emission intensity of Figure 6. Hence, we can draw a reasonable conclusion that Sr^{2+} doping increases the crystallinity. Secondly, the drift of the diffraction peaks (Figure 1(c)) and the change of the cell parameters (Figure 1(d)) indicate that the introduction of Sr^{2+} ions leads to the decrease of the local crystal field symmetry around Er^{3+} ions. This is also

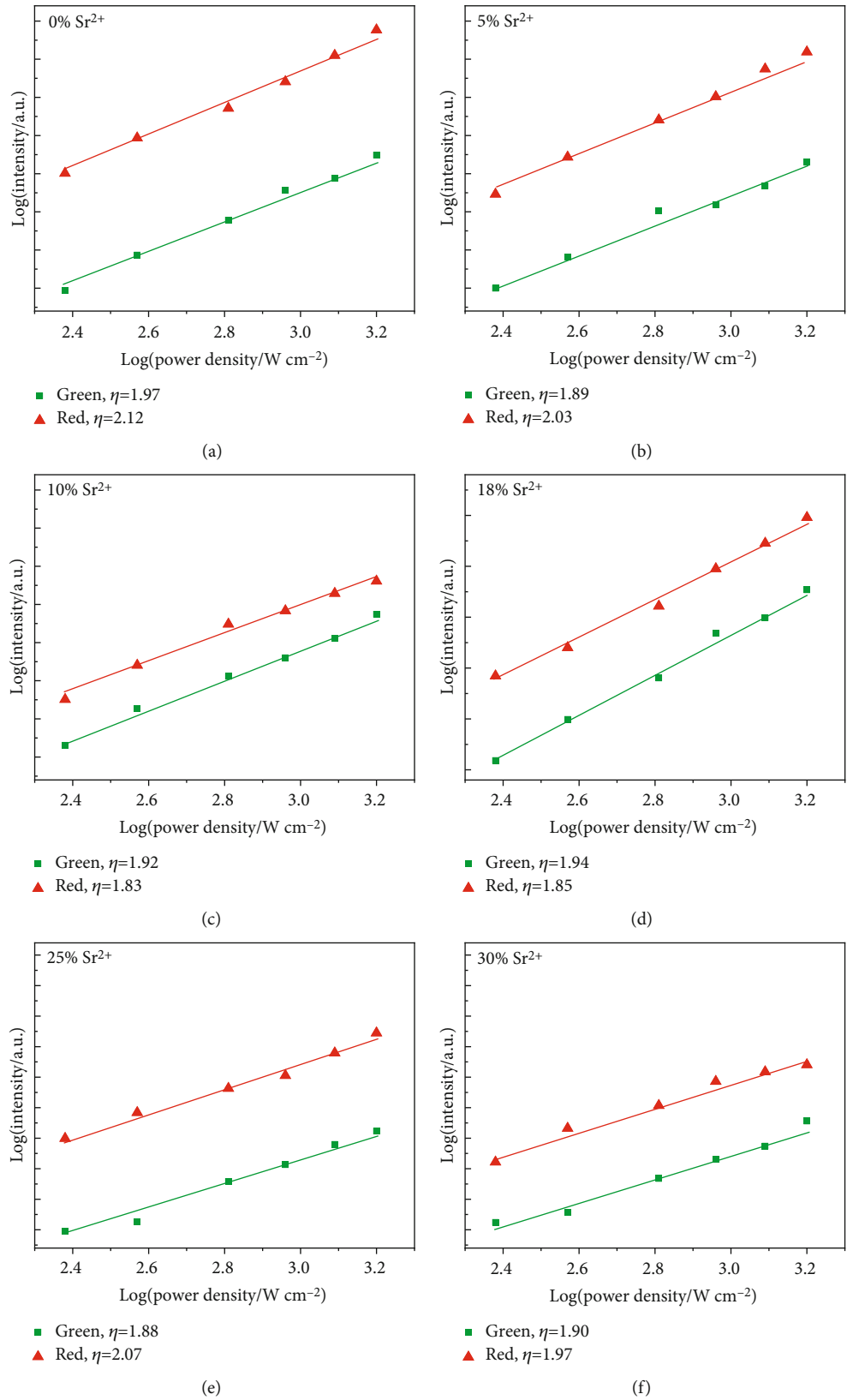

Figure 7: Log-log of the UC emission intensity against laser excitation power for $NaLuF_4$:6%Er^{3+}, x% Sr^{2+} samples with x = 0, 5, 10, 18, 25, 30 (color figure online).

considered to be the reason for boosting the UC emission intensity. However, if excessive Sr^{2+} ions are incorporated into the host matrices, the symmetry around the Er^{3+} activator will gradually become better, resulting in a decrease in emission efficiency. Eventually, the UC emission intensity is reduced when the Sr^{2+} amount surpasses 18%. The reasons are twofold. On the one hand, high concentration of dopant may damage the unit cell structure of the β-$NaLuF_4$:6%Er^{3+} microcrystals and cause the formation of impurity phase SrF_2. On the other hand, high Sr^{2+} doping leads to excessive F^- vacancies, which acts as the quenching center in the β-$NaLuF_4$:6%Er^{3+} microcrystals. This kind of quenching effect was reported by Cong et al.'s group in the Zn^{2+}-doped $NaGdF_4$:Yb^{3+}, Er^{3+} nanoparticles [28]. Finally, from the morphological point of view, 18% Sr^{2+} concentration is an optimal concentration. As can be seen from Figure 2, the microtubes without any irregular particles are obtained at this time. Under the excitation of 980 nm, the UC emission intensities of hexagonal microtubes and hexagonal microprisms are different, for the following reasons: when infrared light is irradiated onto the microtubes, the electric vectors spread along the surface and inner wall at the same time. When infrared light is irradiated on the microprisms, the electric vectors only spread along the surface. Therefore, under the same power of 980 nm infrared laser, the UC emission intensity of hexagonal microtubes is stronger than that of microprisms.

To illustrate the number of incident photons responsible for the upconversion process, the relation of UCL intensities versus excitation power density was drawn. For the unsaturated upconversion process, the number (n) of photons needed to emit a green or red photon can be obtained using the following equation [29, 30]:

$$I_{em} \propto P^n, \tag{2}$$

where n is the number of pump photons absorbed, P is the excitation power intensity, and I_{em} is the emission intensity. From the double logarithmic plots of the emission intensity as a function of the excitation power (Figure 7), we can see that the 544 nm green emission and 655 nm red emission are ascribed to two-photon upconversion processes. The addition of Sr^{2+} ion cannot absorb 980 nm photons or transfer energy to Er^{3+}. But it is worth noting that the value of n changes slightly with the change of the concentration of Sr^{2+} ions and is smaller than that of Sr^{2+}-free samples. It may be due to the fact that the upconversion process is relatively easy to saturate in $NaLuF_4$ MCs doped with Sr^{2+} ions [31]. Another subtle difference is the number of photons needed for the 544 nm upconversion and that of 655 nm. The main reason is that electrons require steps to reach the $^4F_{9/2}$ state than the $^4S_{3/2}$ and $^2H_{11/2}$ states, and this will deplete more photons. So the 655 nm upconversion emission process will need more photons. According to the theoretical analysis, the possible upconversion routes are displayed in Figure 8, which lists the relevant energy levels of Er^{3+} as well as the emission processes. The 980 nm laser can excite an Er^{3+} ion to $^4F_{7/2}$. Through nonradiative transitions, the electrons of Er^{3+} at $^4F_{7/2}$ relax to $^2H_{11/2}$, $^4S_{3/2}$, or $^4F_{9/2}$ and then transfer back to the ground state $^4I_{15/2}$ and in the meanwhile generate luminescence at 526 nm, 544 nm, and 655 nm.

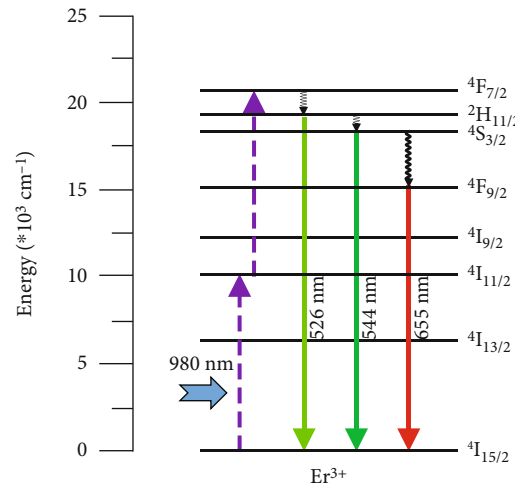

Figure 8: Proposed upconversion mechanism under 980 nm laser excitation.

4. Conclusions

In summary, $NaLuF_4$: Er^{3+} hexagonal microtubes doped with different concentrations of Sr^{2+} ions have been synthesized via a simple hydrothermal method. We systematically investigate the crystal structure, morphology, and UCL enhancement of hexagonal $NaLuF_4$: Er^{3+}. With the increase of Sr^{2+} dosage, the length of $NaLuF_4$ hexagonal microtubes decreases and the morphologies change from hexagonal microtubes to hexagonal prisms. Extending the reaction time, $NaLuF_4$ hexagonal microtubes have undergone a typical Ostwald's ripening. At the optimized concentration (18%) of Sr^{2+} ions, the green and red upconversion emissions are strengthened by 5.8 times and 4.4 times compared to that of Sr^{2+}-free samples. A possible mechanism of upconversion emission enhancement has been identified. All the above results suggest that $NaLuF_4$: Er/Sr microphosphors have broad application prospects in the design and fabrication of high-brightness displays.

Data Availability

The data used to support the findings of this study are available from the corresponding author upon request.

Conflicts of Interest

The authors declare that they have no conflicts of interest.

Acknowledgments

This work was supported by Provincial Natural Foundation of Anhui Province (No. 1808085QF197, No. 1808085MF169), Natural Science Research Project of Anhui Universities of Science and Technology (No. QN201501),

and Ph.D. Research Fund of Anhui Universities of Science and Technology.

References

[1] J. Zhou, Q. Liu, W. Feng, Y. Sun, and F. Li, "Upconversion luminescent materials: advances and applications," *Chemical Reviews*, vol. 115, no. 1, pp. 395–465, 2014.

[2] G. B. Shan and G. P. Demopoulos, "Near-infrared sunlight harvesting in dye-sensitized solar cells via the insertion of an upconverter-TiO_2 nanocomposite layer," *Advanced Materials*, vol. 22, no. 39, pp. 4373–4377, 2010.

[3] Y. Y. Cheng, B. Fückel, R. W. MacQueen et al., "Improving the light-harvesting of amorphous silicon solar cells with photochemical upconversion," *Energy & Environmental Science*, vol. 5, no. 5, pp. 6953–6959, 2012.

[4] F. Wang, D. Banerjee, Y. Liu, X. Chen, and X. Liu, "Upconversion nanoparticles in biological labeling, imaging, and therapy," *Analyst*, vol. 135, no. 8, pp. 1839–1854, 2010.

[5] P. Zhang, W. Steelant, M. Kumar, and M. Scholfield, "Versatile photosensitizers for photodynamic therapy at infrared excitation," *Journal of the American Chemical Society*, vol. 129, no. 15, pp. 4526-4527, 2007.

[6] S. Zhou, K. Deng, X. Wei et al., "Upconversion luminescence of $NaYF_4$: Yb^{3+}, Er^{3+} for temperature sensing," *Optics Communications*, vol. 291, pp. 138–142, 2013.

[7] L. Lei, D. Chen, Y. Han et al., "Modifying the size and uniformity of upconversion Yb/Er: $NaGdF_4$ nanocrystals through alkaline-earth doping," *Nanoscale*, vol. 5, no. 22, pp. 11298–11305, 2013.

[8] J. Wang, T. Wei, X. Li et al., "Near-infrared-light-mediated imaging of latent fingerprints based on molecular recognition," *Angewandte Chemie, International Edition*, vol. 53, no. 6, pp. 1616–1620, 2014.

[9] C. Wang, H. Tao, L. Cheng, and Z. Liu, "Near-infrared light induced in vivo photodynamic therapy of cancer based on upconversion nanoparticles," *Biomaterials*, vol. 32, no. 26, pp. 6145–6154, 2011.

[10] X. Liu, M. Zheng, X. Kong et al., "Separately doped upconversion-C60 nanoplatform for NIR imaging-guided photodynamic therapy of cancer cells," *Chemical Communications*, vol. 49, no. 31, pp. 3224–3226, 2013.

[11] K. M. L. Taylor, A. Jin, and W. Lin, "Surfactant-assisted synthesis of nanoscale gadolinium metal-organic frameworks for potential multimodal imaging," *Angewandte Chemie, International Edition*, vol. 47, no. 40, pp. 7722–7725, 2008.

[12] Z. Chen, H. Chen, H. Hu et al., "Versatile synthesis strategy for carboxylic acid–functionalized upconverting nanophosphors as biological labels," *Journal of the American Chemical Society*, vol. 130, no. 10, pp. 3023–3029, 2008.

[13] F. Wang and X. Liu, "Recent advances in the chemistry of lanthanide-doped upconversion nanocrystals," *Chemical Society Reviews*, vol. 38, no. 4, pp. 976–989, 2009.

[14] Y. Han, C. Gao, Y. Wang et al., "Spatially confined luminescence process in tip-modified heterogeneous-structured microrods for high-level anti-counterfeiting," *Physical Chemistry Chemical Physics*, vol. 20, no. 14, pp. 9516–9522, 2018.

[15] Y. Han, C. Gao, S. Li, and Z. Jiang, "Manipulating emissions of an intensive red-emitting $NaLuF_4$:Yb/Er microrod by controlling its temporal behaviors," *Journal of Alloys and Compounds*, vol. 838, article 155610, 2020.

[16] F. Shi, J. Wang, X. Zhai, D. Zhao, and W. Qin, "Facile synthesis of β- $NaLuF_4$: Yb/Tm hexagonal nanoplates with intense ultraviolet upconversion luminescence," *CrystEngComm*, vol. 13, no. 11, pp. 3782–3787, 2011.

[17] Y. Li, Y. Dong, T. A. Tuerxun·Aidilibike, X. Liu, J. Guo, and W. Qin, "Growth phase diagram and upconversion luminescence properties of $NaLuF_4$: Yb^{3+}/Tm^{3+}/Gd^{3+} nanocrystals," *RSC Advances*, vol. 7, no. 70, pp. 44531–44536, 2017.

[18] J. Yang, L. Song, X. Wang et al., "A facile route to the controlled synthesis of β-$NaLuF_4$: Ln^{3+} (Ln = Eu, Tb, Dy, Sm, Tm, Ho) phosphors and their tunable luminescence properties," *CrystEngComm*, vol. 20, no. 33, pp. 4763–4770, 2018.

[19] H. Lin, X. Yan, J. Zheng, C. Dai, and Y. Chen, "Upconversion luminescence and Visible-Infrared Properties of β-NaLuF4:Er3+ Microcrystals Synthesized by the Surfactant-Assisted Hydrothermal Method," *Journal of Nanomaterials*, vol. 2014, Article ID 903208, 11 pages, 2014.

[20] J. Sun, H. Hao, W. Xu, Y. Song, Y. Wang, and X. Zhang, "Manipulation of microstructures and the stability of white emissions in $NaLuF_4$: Yb^{3+}, Ho^{3+}, Tm^{3+} upconversion crystals," *Optical Materials Express*, vol. 8, no. 4, pp. 1043–1057, 2018.

[21] Q. Qiang, S. du, X. Ma, W. Chen, G. Zhang, and Y. Wang, "A temperature sensor based on the enhanced upconversion luminescence of Li^+ doped $NaLuF_4$:Yb^{3+},Tm^{3+}/Er^{3+} nano/microcrystals," *Dalton Transactions*, vol. 47, no. 26, pp. 8656–8662, 2018.

[22] S. Sinha, A. Mondal, K. Kumar, and H. C. Swart, "Enhancement of upconversion emission and temperature sensing of paramagnetic $Gd_2Mo_3O_9$: Er^{3+}/Yb^{3+} phosphor via Li^+/Mg^{2+} co-doping," *Journal of Alloys and Compounds*, vol. 747, pp. 455–464, 2018.

[23] L. Lei, D. Chen, J. Xu, R. Zhang, and Y. Wang, "Highly intensified upconversion luminescence of Ca^{2+}-doped Yb/Er:-$NaGdF_4$ Nanocrystals prepared by a solvothermal route," *Chemistry, an Asian Journal*, vol. 9, no. 3, pp. 728–733, 2014.

[24] X. Wang, X. Zhang, Y. Wang et al., "Comprehensive studies of the Li^+ effect on $NaYF_4$: Yb/Er nanocrystals: morphology, structure, and upconversion luminescence," *Dalton Transactions*, vol. 46, no. 28, pp. 8968–8974, 2017.

[25] A. Zhou, F. Song, Y. Han, F. Song, D. Ju, and X. Wang, "Simultaneous size adjustment and upconversion luminescence enhancement of β-$NaLuF_4$: Yb^{3+}/Er^{3+}, Er^{3+}/Tm^{3+} microcrystals by introducing Ca^{2+} for temperature sensing," *CrystEngComm*, vol. 20, no. 14, pp. 2029–2035, 2018.

[26] Q. Shao, H. Zhang, J. Dai et al., "Preparation, growth mechanism, size manipulation and near-infrared luminescence enhancement of β-NaYF4:Nd^{3+} microcrystals via Ca^{2+} doping," *CrystEngComm*, vol. 21, no. 4, pp. 741–748, 2019.

[27] Z. Huang, Y. Yang, L. Gong, M. Ma, and C. Xu, "Sr^{2+} and Tb^{3+} doping tuning the size, morphology, and photoluminescence of $NaCeF_4$ nanorods via solvothermal method," *Chemical Engineering Journal*, vol. 286, pp. 602–609, 2016.

[28] T. Cong, Y. Ding, J. Liu, H. Zhao, and X. Hong, "Synthesis and optical properties of Zn^{2+} doped $NaYF_4$: Yb^{3+}, Er^{3+} upconversion nanoparticles," *Materials Letters*, vol. 165, pp. 59–62, 2016.

[29] M. Pollnau, D. R. Gamelin, S. R. Lüthi, H. U. Güdel, and M. P. Hehlen, "Power dependence of upconversion luminescence in lanthanide and transition-metal-ion systems," *Physical Review B*, vol. 61, no. 5, pp. 3337–3346, 2000.

[30] K. Du, X. Xu, S. Yao et al., "Enhanced upconversion luminescence and controllable phase/shape of NaYF4:Yb/Er crystals through Cu^{2+} ion doping," *CrystEngComm*, vol. 20, no. 14, pp. 1945–1953, 2018.

[31] X. Deng, M. Yu, X. Zhou, Z. Xia, X. Chen, and S. Huang, "Highly bright and sensitive thermometric $LiYF_4$:Yb, Er upconversion nanocrystals through Mg^{2+} tridoping," *Journal of Materials Science: Materials in Electronics*, vol. 31, no. 4, pp. 3415–3425, 2020.